
PET Imaging of Regional ^{18}F -FDG Uptake and Lung Function After Cigarette Smoke Inhalation

Tobias Schroeder¹, Marcos F. Vidal Melo¹, Guido Musch¹, R. Scott Harris², Tilo Winkler¹, and Jose G. Venegas¹

¹Department of Anesthesia and Critical Care, Massachusetts General Hospital and Harvard Medical School, Boston, Massachusetts; and ²Pulmonary and Critical Care Unit, Massachusetts General Hospital and Harvard Medical School, Boston, Massachusetts

Cigarette smoke is thought to promote local lung inflammation that leads to lung dysfunction. Lung neutrophilic inflammation is known to result in increased pulmonary uptake of ^{18}F -FDG. Using a sheep model of localized exposure to cigarette smoke, in this study we tested whether PET-imaged changes in regional intrapulmonary distribution of ^{18}F -FDG uptake are related to changes in regional lung function as assessed with the infused ^{13}NN -saline method. **Methods:** Five anesthetized, mechanically ventilated sheep were exposed to unilateral inhalation of smoke from 10 tobacco cigarettes while the contralateral lung was ventilated with smoke-free gas. Two hours after the exposure, regional gas content was measured from a transmission scan; regional ventilation, perfusion, and shunt were measured from the kinetics of ^{13}NN -saline; and regional ^{18}F -FDG influx constant (K_i) was calculated with the Patlak algorithm applied at a voxel-by-voxel level. **Results:** K_i was higher and more heterogeneous in the smoke-exposed lungs than in the control lungs ($P < 0.05$). Spatial heterogeneity of K_i and impairment in regional lung function were quite variable among animals despite similar levels of smoke exposure. However, increases in mean K_i correlated linearly with its spatial heterogeneity (Spearman correlation, $r_s = 0.94$), and the highest levels of regional K_i in smoke-exposed lungs and control lungs correlated with regional shunt fraction ($r_s = 0.78$). Also, the heterogeneity of the ventilation-perfusion (\dot{V}/\dot{Q}) distribution of the smoke-exposed lungs was 10 times greater than that of the control lungs but correlated strongly with that of the control lungs ($r = 0.998$). **Conclusion:** Substantial interanimal variability and spatial heterogeneity in lung function and ^{18}F -FDG uptake seem to characterize the response to smoke exposure. The highest levels of local ^{18}F -FDG uptake were associated with differences in \dot{V}/\dot{Q} matching and shunt fraction among animals. The data also suggest that preexisting heterogeneity in \dot{V}/\dot{Q} could have been responsible for the large interanimal variability by affecting the heterogeneity and strength of the acute response to smoke inhalation.

Key Words: positron emission tomography; FDG; pulmonary gas exchange; inflammation; smoke inhalation injury

J Nucl Med 2007; 48:413–419

Inhalation of smoke promotes pulmonary inflammation by inducing chemotaxis, retention, and activation of neutrophils and macrophages (1,2). The inflammatory process is thought to be essential in the development of lung injury and in the ensuing impairment of lung function (3,4). However, the pathologic response to smoke appears to vary among individuals, at least as judged from the small number of smoke-exposed patients in whom acute lung injury develops (5) and from the limited fraction of cigarette smokers in whom chronic obstructive pulmonary disease develops (6,7). In fact, a recent report stressed the importance of the inter- and intrasubject variability of chronic obstructive pulmonary disease (8).

Acute lung injury by severe smoke exposure has been shown to be spatially heterogeneous (9), but there are only limited data on the topographic distribution of inflammation and its association with impaired regional lung function after smoke inhalation. Such information could be valuable in helping us understand the mechanism of smoke-related lung injury, the crucial role that neutrophils play in this condition (10), and the intersubject variability in the response to smoke.

PET offers the potential for combining noninvasive regional assessments of inflammation and lung function. Recent studies have shown that acute pulmonary neutrophilic inflammation results in increased pulmonary uptake of ^{18}F -FDG measured over the lung field (11) or regions of interest (12,13). We have used tracer kinetic modeling of intravenously injected ^{13}NN -saline to assess regional gas exchange in normal and pathologic lungs (14), including acute lung injury after smoke inhalation (9). In the present study, these methods were used to evaluate whether regional pulmonary ^{18}F -FDG uptake was increased in lungs acutely exposed to cigarette smoke, whether that increase was spatially uniform or heterogeneous, and whether intersubject differences in regional ^{18}F -FDG uptake were associated with intersubject differences in functional response to smoke exposure. To accomplish these objectives, we studied an animal model of acute unilateral exposure to cigarette smoke in which the contralateral lung of each animal was used as the control.

Received May 10, 2006; revision accepted Nov. 27, 2006.
For correspondence or reprints contact: Jose G. Venegas, PhD, Massachusetts General Hospital, Department of Anesthesia and Critical Care, CLN 255, 55 Fruit St., Boston, MA 02114.
E-mail: jvenegas@vqpet.mgh.harvard.edu
COPYRIGHT © 2007 by the Society of Nuclear Medicine, Inc.

MATERIALS AND METHODS

Model of Unilateral Pulmonary Smoke Exposure

The Subcommittee on Research Animal Care of the Massachusetts General Hospital approved the study in accordance with the guidelines of the National Institutes of Health. Five female sheep (22–32 kg) were kept fasting for 24 h before the beginning of the experiment. They were then anesthetized, intubated, and mechanically ventilated. A Swan–Ganz catheter (7.5 French) was advanced to the pulmonary artery. The proximal (central venous) port was used for administration of the radioisotopes, and the distal port was used for pulmonary arterial blood sampling. General anesthesia and muscle paralysis were maintained with an infusion of sodium thiopental, fentanyl, and pancuronium. Tidal volume was adjusted to maintain normocapnia and a respiratory rate of 10 breaths per minute. The lungs were isolated with a double-lumen tube, and the tidal volumes to each lung were set to make peak inspiratory pressures equal to those measured before isolation. The left lung was then exposed to cigarette smoke by interposing along the inspiratory limb of the breathing circuit a chamber containing the lit cigarette so that all the inspiratory flow passed through the cigarette (Basic; Philip Morris) until three quarters of the cigarette was consumed. During smoke exposure, the left lung was ventilated with room air whereas the right lung was ventilated with 50% O₂. Between exposures, both lungs were ventilated for 5 min with 100% O₂. After serial exposure to 10 cigarettes, the double-lumen tube was replaced by a single-lumen tube and combined mechanical ventilation was resumed at a respiratory rate and tidal volume equal to those used before smoke exposure: 50% inspired O₂ and a positive end-expiratory pressure of 5 cm of H₂O.

PET Protocols and Tracer Kinetics

Two hours after smoke exposure, each sheep was positioned prone in the PET camera (Scanditronix PC4096; GE Healthcare) with the most caudal slice adjacent to the diaphragm dome to maximize the imaged lung volume (14). The camera collected 15 transverse cross-sectional slices of 6.5-mm thickness over a 9.7-cm-long axial field.

A transmission scan was obtained to correct for tissue attenuation of the emitted photons and to define regions of interest corresponding to lung fields. To assess regional ventilation and perfusion, dynamic emission scanning of the intrapulmonary kinetics of intravenously injected ¹³NN-gas in saline solution was performed as previously described in detail (15). Briefly, starting with a tracer-free lung, ventilation was stopped at the mean lung volume and a bolus of ¹³NN-saline solution (344 ± 96 MBq dissolved in 30 mL) was injected at a rate of 10 mL/s. Simultaneously with the start of the ¹³NN-saline injection, image acquisition was started (8 images acquired for 2.5 s each, 10 images for 10 s, and 4 images for 30 s) to measure the kinetics of infused ¹³NN during 60 s of apnea and during the ensuing 3 min of washout by ventilation after breathing resumed.

At least 30 min after the ¹³NN injection, 370 MBq of ¹⁸F-FDG were injected at a constant rate over 1 min. By this time, the ¹³NN activity had been cleared from the lungs by radioactive decay (half-life, 9.96 min) and by ventilation. The acquisition protocol for ¹⁸F-FDG consisted of 32 consecutive images for a total of 75 min (6 × 30 s, 7 × 1 min, 15 × 2 min, 1 × 5 min, and 3 × 10 min). ¹⁸F-FDG activity in blood plasma as a function of time (C_p(t)) was measured from sequential 1-mL samples of pulmonary arterial blood in a well counter cross-calibrated with the PET

camera. For the first 4.5 min, the time points of blood sampling were synchronized with the time points of the PET frames. At later times, the plasma measurements were linearly interpolated and values coinciding with the PET frames were extracted from the interpolated data.

PET images were reconstructed with the standard convolution-backprojection algorithm and then filtered with an in-plane, low-pass Hanning kernel and a 2-point moving average in the z-direction, yielding an effective volumetric resolution of 2.2 cm³ (14).

Regional Ventilation (\dot{V}_r), Perfusion (\dot{Q}_r), Gas Fraction (F_{gas}), and Shunt Fraction

¹³NN tracer kinetics were analyzed at the voxel level to compute intraregional specific ventilation ($s\dot{V}_r$), defined as ventilation per unit of gas volume, perfusion (\dot{Q}_r), and the ventilation–perfusion ratio (\dot{V}/\dot{Q}), using a method similar to one previously described (14). A voxel was classified as homogeneous when a semilog plot of the tracer concentration during washout approached linearity and was treated as a single compartment whether ventilating or not (gas trapping). A voxel was classified as heterogeneous when the semilog washout plot was curvilinear. In this case, the voxel was analyzed as being composed of 2 compartments, either both ventilating or one ventilating and the other gas-trapping. For each compartment, ventilation (\dot{V}_r) was calculated as the product of $s\dot{V}_r$, measured as the reciprocal of the time constant of the exponential washout of the compartment, and a corresponding gas volume. In homogeneous voxels, gas volume was estimated as the product of the voxel volume and its gas fraction (F_{gas}) obtained from the transmission scan (16). In heterogeneous voxels, the gas volume was partitioned between the 2 compartments in proportion to the blood flow fraction of the compartment. The fraction of blood flow to each compartment was estimated from the relative tracer activity of the compartment at the beginning of the washout of infused ¹³NN. In addition, the fractional tissue content (F_{tis}) was calculated for each voxel as $F_{\text{tis}} = 1 - F_{\text{gas}}$.

As described previously (14), the average regional tracer activity measured during the plateau phase of apnea (Fig. 1A) is proportional to \dot{Q}_r . From that measurement, \dot{Q}_r , expressed as a fraction of cardiac output, was calculated as the ratio of the average regional tracer activity during apnea to the injected dose of ¹³NN. The regional shunt fraction for each lung was estimated from the difference between ¹³NN peak activity at the beginning of apnea and the activity at the end of the plateau phase, normalized to the peak (17). This estimate includes blood flow to regions of true right-to-left shunting and regions showing very low \dot{V}/\dot{Q} in combination with a low alveolar gas content.

Values of \dot{V}/\dot{Q} normalized by a blood-flow–weighted mean \dot{V}/\dot{Q} for the imaged lung were grouped into bins of equal log width (0.05) ranging from –2 to 2 and plotted as a function of the corresponding fraction of perfusion in distribution histograms for the smoke-exposed and control lung. The second moment of the perfusion-weighted distribution about its mean on a log scale ($\text{cov}^2(\log \dot{V}/\dot{Q})$) was used to quantify \dot{V}/\dot{Q} heterogeneity in each lung.

¹⁸F-FDG Uptake

The uptake rate of ¹⁸F-FDG was assessed as the influx constant K_i determined from the slope of a Patlak plot, constructed from the tissue and plasma radioactivity (Fig. 1C) (18). To assess the spatial distribution of ¹⁸F-FDG uptake, we applied the method to each voxel, yielding parametric images of local K_i . The linearity

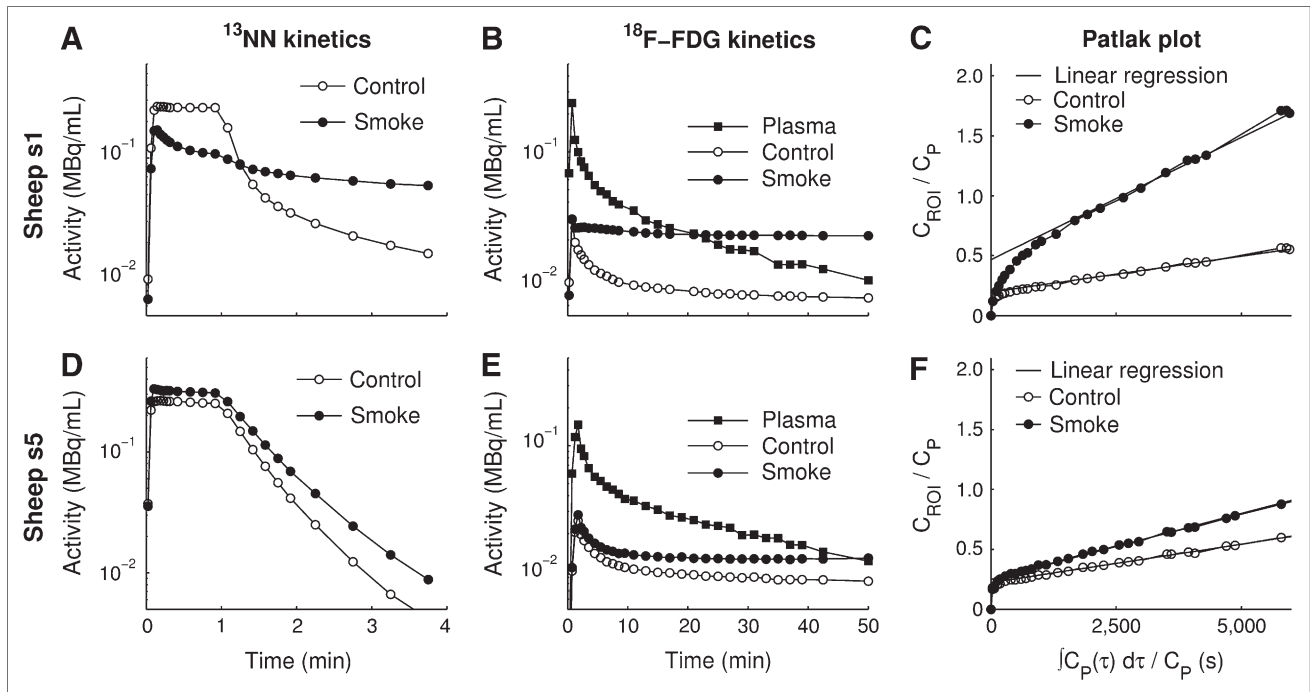


FIGURE 1. Pulmonary tracer kinetics in sheep with largest response to smoke (s1) and sheep with smallest response to smoke (s5). (A and D) Mean lung activity calculated as average of all voxels within each lung after intravenous injection of ^{13}NN -saline. (B and E) Mean lung activity of ^{18}F -FDG and concentration of this tracer in blood plasma. (E and F) Patlak plots generated from ^{18}F -FDG kinetics in C and D. Slope of linear regression of Patlak plots yields ^{18}F -FDG influx constant K_i .

of Patlak plots generated from voxel ^{18}F -FDG kinetics was confirmed by generating images of the Pearson correlation coefficient (r). In addition, we calculated a tissue-normalized K_i (K_i/F_{tis}) by dividing the K_i of each voxel by the corresponding F_{tis} .

To analyze the spatial heterogeneity of K_i , we grouped local values of K_i into bins of equal width ($0.5 \cdot 10^{-3} \text{ min}^{-1}$) ranging from 0 to 0.05 min^{-1} and plotted them as a function of the corresponding fraction of lung volume in a distribution histogram for each lung. From those histograms, the mean and SD of the K_i distribution were calculated for the control and the smoke-exposed lungs. The SD of K_i was used as a measure of spatial heterogeneity. The animals were ranked in descending order according to the SD of the K_i distribution of the smoke-exposed lung (sheep 1 [s1] having the highest value).

The highest local level of metabolic activity ($K_{i,\text{max}}$) was defined as the mean plus 1 SD of the K_i histograms for each lung.

Definition of Lung Fields

Volumetric masks of the imaged lung field were generated with an interactive software tool that allowed combining data from different PET scans. Masks generated by thresholding voxels of aerated lung ($F_{\text{gas}} > 0.28$) were combined with masks generated by thresholding voxels of perfused lung. In this way, aerated regions as well as perfused but poorly aerated (collapsed or flooded) regions were included in the final mask. Masks were designed for each lung; large pulmonary vessels and airways down to the second generation were excluded manually.

Statistics

The correlation between 2 different variables within smoke-exposed or control lungs was assessed with the nonparametric Spearman rank correlation coefficient (r_s), where control and

smoke-exposed lung values were treated as independent measurements. This analysis is insensitive to outliers and does not imply any assumptions about the statistical distribution of the variables. Paired t tests were performed to compare smoke and control measurements. Significance was set at a P value of less than 0.05.

RESULTS

All sheep showed stable hemodynamics and respiratory mechanics at the time of imaging—that is, 2 h after the end of cigarette smoke exposure (Table 1).

Despite similar doses of administered smoke, lung tracer kinetics were quite variable among the sheep, as depicted for 2 extreme cases in Figure 1.

Activity of ^{13}NN either reached a plateau in both lungs immediately after injection (Fig. 1D) or first rose in the smoke-exposed lung to an early peak and then declined to a plateau (Fig. 1A).

TABLE 1

Ventilatory and Cardiovascular Data at Time of Imaging

Parameter	Mean \pm SD
Peak airway pressure (cm H ₂ O)	21.7 \pm 1.4
Wedge pressure (cm H ₂ O)	5.5 \pm 4.1
Pulmonary artery pressure (mm Hg)	18 \pm 1
Mean arterial pressure (mm Hg)	89 \pm 18
Systolic arterial pressure (mm Hg)	112 \pm 16
Diastolic arterial pressure (mm Hg)	79 \pm 18
Heart rate (min ⁻¹)	121 \pm 27

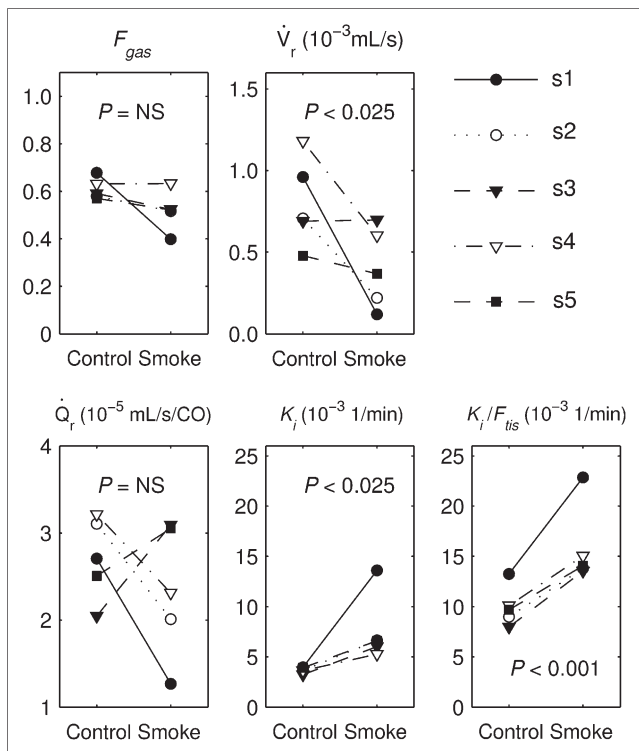


FIGURE 2. Mean values of lung function variables for all 5 sheep (s1–s5) in control and smoke-exposed lungs.

Because of its low solubility in blood (partition coefficient $\lambda_{\text{water/air}} = 0.015$ at 37°C), virtually all infused ^{13}N diffuses across the pulmonary capillaries into the aerated alveolar space at the first pass, where it accumulates in proportion to regional perfusion. In contrast, lung regions that are perfused but not aerated (i.e., shunting) do not retain the tracer during apnea, and in these regions tracer activity decreases exponentially during the latter part of the breath-hold. When breathing resumes, tracer is eliminated from the alveolar airspace by ventilation.

Tracer washout curves ranged from somewhat linear (Fig. 1D) to markedly curvilinear, indicating intraregional ventilation heterogeneity (Fig. 1A), and incomplete tracer washout was observed (Fig. 1A).

In each sheep, the peak of ^{18}F -FDG activity after injection was similar in the smoke-exposed and control lungs (Figs. 1C and 1E). After the peak, ^{18}F -FDG activity dropped toward a plateau with higher activity in the smoke-exposed than in the control lungs.

For average lung values, \dot{V}_r showed significant differences between both lungs (Fig. 2), the difference in F_{gas} and \dot{Q}_r being either moderate (F_{gas}) or variable (\dot{Q}_r). In contrast, differences between lungs in mean K_i and K_i/F_{tis} were consistent, with both variables being significantly higher in the smoke-exposed than in the control lung of 4 sheep and dramatically higher in the smoke-exposed lung of 1 sheep.

Images of regional function variables reflected the variable response in magnitude but also revealed intraregional heterogeneity that was quite variable among the sheep (Fig. 3), ranging from highly heterogeneous in the smoke-exposed lung to only moderately heterogeneous in both lungs. Spatial heterogeneity was also present in images of K_i and K_i/F_{tis} .

Regional histogram analysis mirrored the apparent variability in intraregional heterogeneity (Fig. 4). \dot{V}/\dot{Q} distributions were more heterogeneous in the smoke-exposed than in the control lungs in 4 sheep, but the degree of \dot{V}/\dot{Q} derangement in the smoke-exposed lungs differed among sheep. In the control lungs, K_i histograms were narrow and similar in all sheep. In the smoke-exposed lungs, K_i histograms were broadened and markedly different among sheep. Interestingly, the heterogeneity of K_i distributions in each smoke-exposed lung appeared to parallel that of the \dot{V}/\dot{Q} distributions in the same lung.

Ordinal analysis of the histograms showed that the mean and SD of the K_i distribution correlated ($r_s = 0.939$;

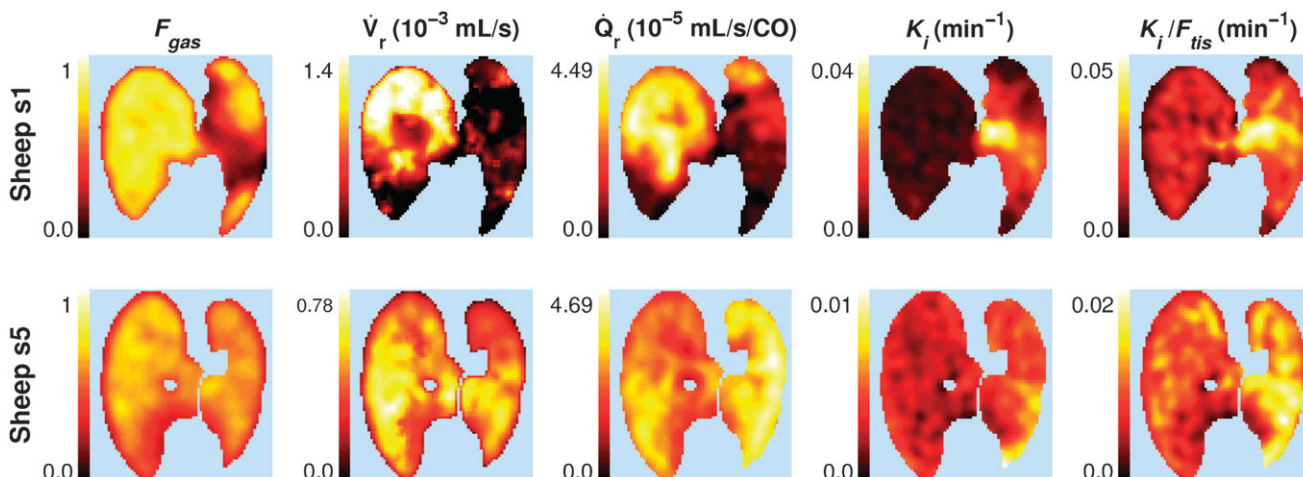


FIGURE 3. Parametric images of lung function variables in sheep with largest response to smoke (s1) and sheep with smallest response to smoke (s5). Smoke-exposed left lung is on right side of each image.

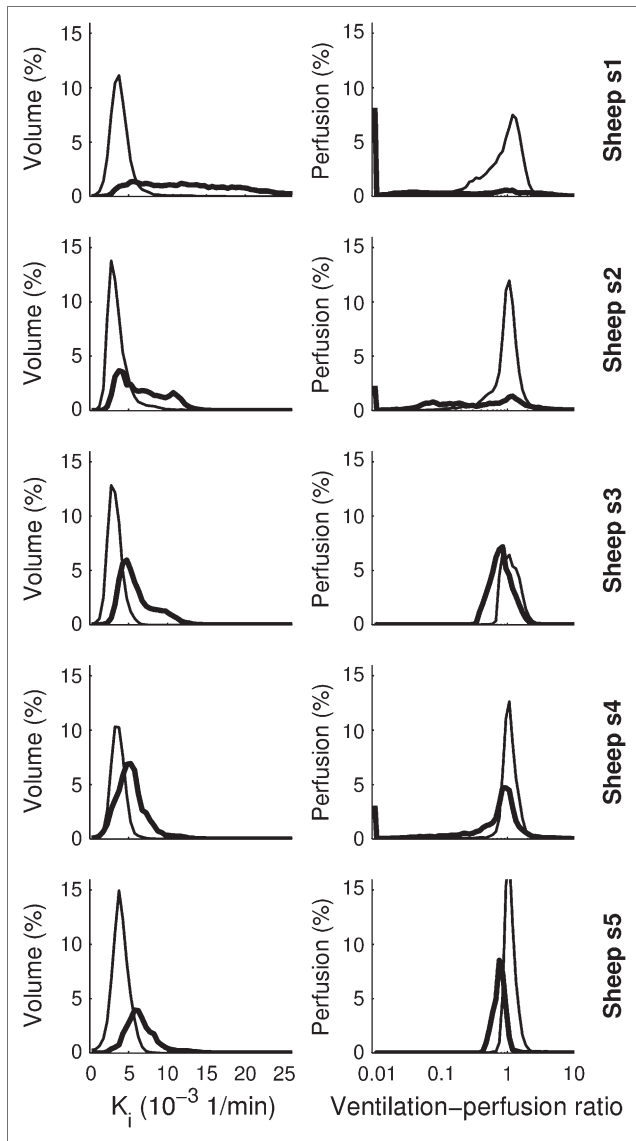


FIGURE 4. (Left) Graphs of K_i in control lung (thin line) and smoke-exposed lung (heavy line) in sheep s1–s5. (Right) Corresponding mean normalized distributions of \dot{V}/\dot{Q} . Animals are ordered by heterogeneity of K_i distribution ($SD(K_i)$) in smoke-exposed lung.

$P < 0.001$) (Fig. 5). Although the results for regional shunting varied, a significant correlation was found between shunting and the highest level of local metabolic activity, $K_{i,max}$ ($r_s = 0.782$; $P < 0.05$) (Fig. 6A). $cov^2(\log \dot{V}/\dot{Q})$ correlated moderately with $K_{i,max}$ (Fig. 6B). In addition, the $cov^2(\log \dot{V}/\dot{Q})$ of the smoke-exposed lung correlated strongly with that of the control lung (Fig. 7) ($r = 0.998$; $P < 0.001$), although smoke and control lung values differed by an order of magnitude and were variable.

DISCUSSION

In this study, we combined tracer kinetic modeling of intravenously injected ^{18}F -FDG and ^{13}N -saline solution to study regional metabolic activity, likely related to pul-

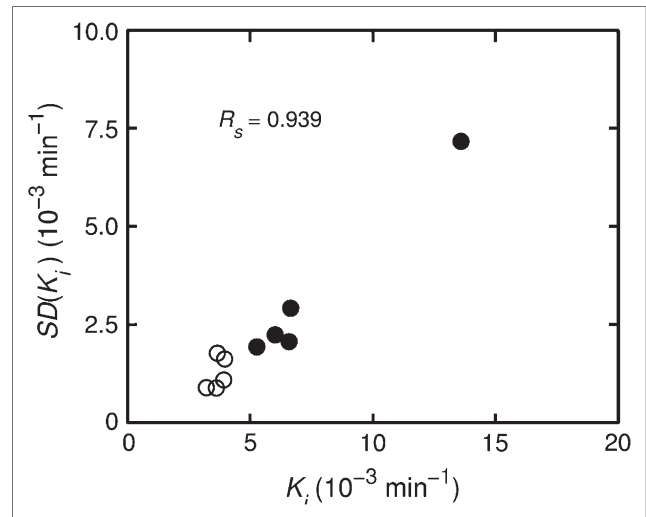


FIGURE 5. Plot of heterogeneity in K_i , $SD(K_i)$, vs. mean K_i in control lung (○) and smoke-exposed lung (●). r_s , Spearman rank correlation coefficient, was calculated from all data points.

monary inflammation, and gas exchange dysfunction after unilateral cigarette smoke inhalation. The results demonstrated an early association of regional gas exchange impairment and regional metabolic activity after acute inhalation of cigarette smoke, despite substantial inter- and intra-animal variability of the response.

The methodologic limitations and assumptions of the ^{13}N -saline method have been detailed in previous publications (15,19). Specifically to this study, we used a unilateral lung exposure model to characterize the regional relationship between changes in ^{18}F -FDG uptake and lung function resulting from smoke inhalation. This model also allowed paired comparisons between exposed and non-exposed lungs in each animal. Animals were given a high

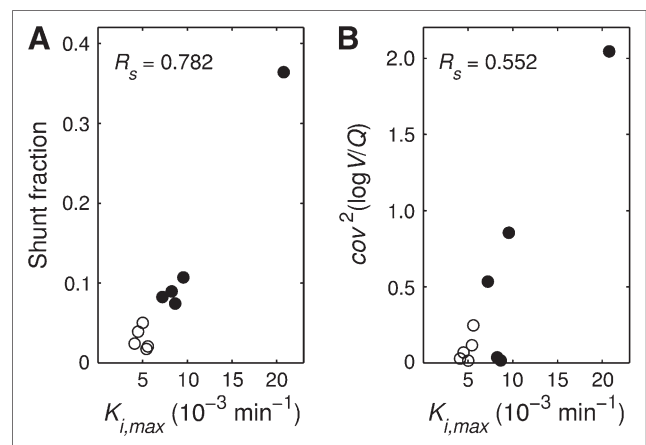


FIGURE 6. Correlation of highest level of local inflammation ($K_{i,max}$) with lung functional parameters within each lung field. (A) Regional shunt fraction plotted against $K_{i,max}$ in control lung (○) and smoke-exposed lung (●). (B) Plot of heterogeneity of \dot{V}/\dot{Q} distribution ($cov^2(\log \dot{V}/\dot{Q})$) in control lung (○) and smoke-exposed lung (●) against $K_{i,max}$.

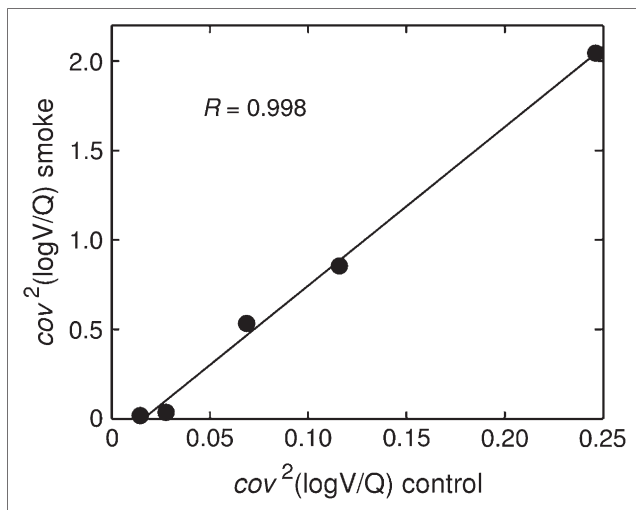


FIGURE 7. $\text{cov}^2(\log \dot{V}/Q)$ in smoke-exposed lung plotted against that in control lung.

dose of localized cigarette smoke thought to promote an inflammatory burden sufficient to cause measurable changes in K_i and regional lung function within 2 h of the exposure. Little is known about the localized toxicity and about the resulting acute inflammatory stimulus of cigarette smoke in the sheep. However, the level of acute smoke exposure in this model could appear higher than that during smoking in a human because the smoke was delivered unilaterally and to a smaller lung. Nevertheless, it is also reasonable to expect that some regions within the heterogeneous lung of a heavy smoker with chronic obstructive pulmonary disease would be subjected to higher local exposure than that expected for a uniform healthy lung.

In a previous study from our group using cotton smoke inhalation, decreases in F_{gas} in dependent lung regions were detected only 4 h after exposure (9). Thus, the lack of a significant change in F_{gas} observed in this study was likely due to the short interval between smoke exposure and measurement and illustrates that mean lung density, unlike ^{18}F -FDG uptake, was not a sensitive indicator of early response to smoke exposure. In contrast, regional ventilation, \dot{V}_r , was significantly reduced in the smoke-exposed lung, a finding that parallels the behavior of dependent lung regions after cotton smoke exposure (9). Regional perfusion in the smoke-exposed lung was not systematically altered in all sheep. However, the 3 sheep with the largest drop in regional ventilation were those showing a reduction in regional perfusion, whereas the 2 animals that showed increases in regional perfusion were those with only minor changes in regional ventilation. We could speculate that although hypoxic pulmonary vasoconstriction may have dominated in the cases of significant reduction in regional ventilation, the release of inflammatory vasodilators predominated when the regional drop in ventilation was low.

We observed significantly higher ^{18}F -FDG uptake in the smoke-exposed lungs than in the control lungs. On the basis

of previous studies demonstrating the relationship between ^{18}F -FDG uptake and inflammation (11–13,20), we presume that the observed increase in ^{18}F -FDG uptake is due to activated neutrophils. However, corroborating histopathologic and biochemical data are needed to ascertain this conjecture.

Patlak analysis has been used in previous studies to compute pulmonary ^{18}F -FDG uptake in large regions of interest (13,20). Our results confirm that voxel-by-voxel Patlak analysis can be applied in the setting of acute smoke exposure. In regions with reduced lung aeration, the increase in regional ^{18}F -FDG uptake could simply have been caused by a change in the number of alveolar units per voxel. Jones et al. used the y-intercept of the Patlak plot as an estimate of initial tracer distribution volume to normalize global lung K_i (20). However, Chen et al. concluded that this normalization did not significantly contribute to signal interpretation in their model of acute lung injury (21). We chose the alternative approach of normalizing regional K_i by the regional tissue fraction F_{tis} obtained from transmission scans. Our results showed that increases in regional ^{18}F -FDG uptake were still substantial when the analysis was based on K_i/F_{tis} , supporting the conclusion that regional metabolic activity increased beyond that expected by a mere change in regional inflation. Finally, F_{tis} can also be increased by the presence of tissue edema, hemorrhage, or transudate, without reflecting an increase in the number of alveolar units per unit of lung volume. Normalization by tissue density in these cases would tend to underestimate K_i . Thus, our observation of higher K_i/F_{tis} ratios in the injured lung than in the nonexposed lung supports an actual increase in ^{18}F -FDG uptake resulting from smoke exposure in that lung and not simply a difference in lung expansion.

The relatively modest increase ($\sim 50\%$) in mean K_i in the smoke-exposed lung is at least partially due to the averaging of regions of high K_i with those of low K_i . Thus, a comparison of merely mean lung values could potentially conceal local increases in ^{18}F -FDG uptake in this type of smoke inhalation injury.

Regional shunt fraction correlated significantly with the index of highest local level of metabolic activity, $K_{i,\text{max}}$, and the \dot{V}/Q histogram of lungs tended to widen with increased $K_{i,\text{max}}$, suggesting a link between excessive local inflammation and functional impairment of regional gas exchange after smoke exposure.

The linear relationship between the mean and SD of the K_i histograms implies that the development of inflammation after smoke inhalation has to be the result of a spatially heterogeneous process. What makes the process heterogeneous is not clear, but the cause could be related to instabilities created by positive feedback mechanisms intrinsic to the inflammatory response. Noteworthy are the substantial variations in the degree and heterogeneity of K_i among the 5 animals despite similar exposures to cigarette smoke. Despite the limited number of animals studied, this variability in heterogeneity could be a key feature of this type of smoke exposure because it was also present in lung

function. In fact, a large interanimal variability in inflammatory response to cigarette smoke is being observed in genetically identical mice (Robin Tuder, written communication, September 28, 2006). However, the small number of our sheep does not allow generalized conclusions.

We found a high correlation between $cov^2(\log \dot{V}/\dot{Q})$ in the smoke-exposed and nonexposed lungs for each animal. There are 2 potential and mutually exclusive explanations for this result. First, if the nonexposed lung is thought of as representing the condition of the lungs at baseline, heterogeneity in lung function before exposure could have affected the extent to which gas exchange was impaired by smoke. Another potential explanation is that the local exposure to smoke in one lung triggered a systemic release of mediators that affected the \dot{V}/\dot{Q} heterogeneity in the opposite lung. The remarkable similarity of K_i distributions in the nonexposed lungs of all animals and the weak correlation between $K_{i,max}$ and $cov^2(\log \dot{V}/\dot{Q})$ among nonexposed lungs suggest that the second explanation is less likely. Therefore, variable heterogeneity in \dot{V}/\dot{Q} before, and thus during, smoke exposure could have been responsible for the large interanimal variability in the severity of \dot{V}/\dot{Q} mismatch after exposure. Whether the nonexposed lung truly represents a baseline control for the smoke exposed one requires further investigation, including scans to evaluate potential baseline abnormalities in both lungs.

CONCLUSION

Acute exposure to cigarette smoke leads to heterogeneously distributed lung metabolic activity and \dot{V}/\dot{Q} mismatch. The highest level of local ^{18}F -FDG uptake is associated with derangement of ventilation and increase in shunt fraction. Interanimal variability and spatial heterogeneity in lung function and metabolic activity seem to characterize this type of smoke exposure, at least as judged from our limited number of studies. We speculate that preexisting heterogeneity in \dot{V}/\dot{Q} could have affected the heterogeneity and strength of the inflammatory response after smoke exposure.

ACKNOWLEDGMENTS

We thank Dr. Rubin Tuder for his comments, and we thank the staff of the Division of Nuclear Medicine at Massachusetts General Hospital. Funding was provided by grants HL-56879 and HL-068011 from the National

Institutes of Health. One of the authors was supported in part by the German Academic Exchange Service (DAAD).

REFERENCES

1. van der Vaart H, Postma DS, Timens W, ten Hacken NH. Acute effects of cigarette smoke on inflammation and oxidative stress: a review. *Thorax*. 2004;59:713–721.
2. MacNee W, Wiggs B, Belzberg AS, Hogg JC. The effect of cigarette smoking on neutrophil kinetics in human lungs. *N Engl J Med*. 1989;321:924–928.
3. Traber DL, Linares HA, Herndon DN, Prien T. The pathophysiology of inhalation injury: a review. *Burns Incl Therm Inj*. 1988;14:357–364.
4. Basadre JO, Sugi K, Traber DL, Niehaus GD, Herndon DN. The effect of leukocyte depletion on smoke inhalation injury in sheep. *Surgery*. 1988;104:208–215.
5. Ryan CM, Schoenfeld DA, Thorpe WP, Sheridan RL, Cassem EH, Tompkins RG. Objective estimates of the probability of death from burn injuries. *N Engl J Med*. 1998;338:362–366.
6. Devereux G. ABC of chronic obstructive pulmonary disease: definition, epidemiology, and risk factors. *BMJ*. 2006;332:1142–1144.
7. Chapman KR, Mannino DM, Soriano JB, et al. Epidemiology and costs of chronic obstructive pulmonary disease. *Eur Respir J*. 2006;27:188–207.
8. Gamble E, Qiu Y, Wang D, et al. Variability of bronchial inflammation in chronic obstructive pulmonary disease: implications for study design. *Eur Respir J*. 2006;27:293–299.
9. Willey-Courand DB, Harris RS, Galletti GG, Hales CA, Fischman A, Venegas JG. Alterations in regional ventilation, perfusion, and shunt after smoke inhalation measured by PET. *J Appl Physiol*. 2002;93:1115–1122.
10. Dhami R, Gilks B, Xie C, Zay K, Wright JL, Churg A. Acute cigarette smoke-induced connective tissue breakdown is mediated by neutrophils and prevented by alpha1-antitrypsin. *Am J Respir Cell Mol Biol*. 2000;22:244–252.
11. Chen DL, Schuster DP. Positron emission tomography with [^{18}F]fluorodeoxyglucose to evaluate neutrophil kinetics during acute lung injury. *Am J Physiol Lung Cell Mol Physiol*. 2004;286:L834–L840.
12. Jones HA, Schofield JB, Krausz T, Boobis AR, Haslett C. Pulmonary fibrosis correlates with duration of tissue neutrophil activation. *Am J Respir Crit Care Med*. 1998;158:620–628.
13. Chen DL, Rosenbluth DB, Mintun MA, Schuster DP. FDG-PET imaging of pulmonary inflammation in healthy volunteers after airway instillation of endotoxin. *J Appl Physiol*. 2006;100:1602–1609.
14. Vidal Melo MF, Layfield D, Harris RS, et al. Quantification of regional ventilation-perfusion ratios with PET. *J Nucl Med*. 2003;44:1982–1991.
15. Mijailovich SM, Treppo S, Venegas JG. Effects of lung motion and tracer kinetics corrections on PET imaging of pulmonary function. *J Appl Physiol*. 1997;82:1154–1162.
16. Harris RS, Willey-Courand DB, Head CA, Galletti GG, Call DM, Venegas JG. Regional VA, Q, and VA/Q during PLV: effects of nitroprusside and inhaled nitric oxide. *J Appl Physiol*. 2002;92:297–312.
17. Galletti GG, Venegas JG. Tracer kinetic model of regional pulmonary function using positron emission tomography. *J Appl Physiol*. 2002;93:1104–1114.
18. Patlak CS, Blasberg RG. Graphical evaluation of blood-to-brain transfer constants from multiple-time uptake data: generalizations. *J Cereb Blood Flow Metab*. 1985;5:584–590.
19. Melo MF, Harris RS, Layfield JD, Venegas JG. Topographic basis of bimodal ventilation-perfusion distributions during bronchoconstriction in sheep. *Am J Respir Crit Care Med*. 2005;171:714–721.
20. Jones HA, Sriskandan S, Peters AM, et al. Dissociation of neutrophil emigration and metabolic activity in lobar pneumonia and bronchiectasis. *Eur Respir J*. 1997;10:795–803.
21. Chen DL, Mintun MA, Schuster DP. Comparison of methods to quantitate ^{18}F -FDG uptake with PET during experimental acute lung injury. *J Nucl Med*. 2004;45:1583–1590.